IIETA International Information and Engineering Technology Association
Advancing the World of Information and Engineering

Mathematical Modelling of Engineering Problems
Vol. 12, No. 7, July, 2025, pp. 2447-2455
Journal homepage: http://iieta.org/journals/mmep

Combined Effect of Heat Source and Pressure in an Unsteady MHD Flow with Chemical Reaction Through an Infinite Oscillating Vertical Porous Surface

Devi Annadurai, Sivakami Lakshminathan*

Department of Mathematics and Statistics, FSH, SRM Institute of Science and Technology, Kattankulathur 603203, Chengalpattu, Tamil Nadu, India

Corresponding Author Email: sivakaml@srmist.edu.in

https://doi.org/10.18280/mmep.120723

Received: 23 March 2025
Revised: 25 May 2025
Accepted: 4 July 2025
Available online: 31 July 2025

Keywords:
pressure gradient, heat source, magnetohydrodynamic (MHD), porous medium, chemical reaction parameter

ABSTRACT

In this study, heat source, pressure gradient, and chemical reaction are investigated in the analytical solution of an unsteady magnetohydrodynamic fluid with heat and mass transfer along a vertical oscillatory surface under the porous medium. This study also investigates the temperature and concentration along with velocity, closer to the surface over time t>0. The Laplace transformation procedure has been implemented for resolving the governing terms of the flow, yielding solutions for temperature, concentration, and velocity. Significant factors that affect velocity, temperature, and concentration—including the Schmidt number, thermal Grashof number, and solutal Grashof number are analysed and results are illustrated graphically using MATLAB. The results obtained here are consistent with the previously published work. From the current investigation, it is reported that velocity decreases with a rise in Hartmann's number (M). As the chemical reaction Kr rises, the velocity has a retarding effect, whereas the concentration increases, and while the heat source (Qs) increases corresponding velocity and temperature both are increasing. As pressure gradient P increases, velocity decreases gradually.

1. INTRODUCTION

An examination of free convection and heat transfer in permeable flows responsive to magnetism has garnered substantial attention due to its extensive scientific and technological implications. Film vaporization in combustion systems, surface ablation procedures, and cooling techniques for rocket boosters and re-entry vehicles are some examples of these uses. Furthermore, flows in permeable materials are essential in numerous engineering and geophysical fields, including filtration and purification in chemical processes, the examination of groundwater circulation in agricultural engineering, and the assessment of fluid dynamics in petroleum reservoirs encompassing oil, natural gas, and water. Because of this, many studies have focused on magnetohydrodynamic (MHD) free convection, weight transfer on permeable surfaces with diverse shapes.

Unsteady MHD flow in porous medium over an oscillating vertical plate has been thoroughly examined by Krishna et al. [1], who analysed heat and mass transfer effects in such a configuration. Krishna and Chamkha [2] and Krishna [3] explored the impacts of hall and ion slip currents in rotating nanofluid and Jeffreys fluid flow respectively. The inclusion of ion slip and porous effects in a nanofluid setting was extended by Krishna and Chamkha [4], while heat source and chemical reaction effects in viscoelastic MHD flows were discussed by Krishna and Jyothi [5]. These studies provide fundamental insights into how electromagnetic and reactive phenomena influence transport processes.

Khanam and Ahmed [6] and Anand Kumar et al. [7] mined the interplay of thermal radiation, mass diffusion, and chemical kinetics in porous channels, showing how reaction rates can drastically modify concentration profiles. The incorporation of thermal radiation, often modeled using the Rosseland approximation, has been addressed by Merkin et al. [8] and Ahammad et al. [9]. Hari Babu [10] focused on chemically reactive Casson and viscous fluids in porous setups, illustrating how increasing the reaction parameter leads to significant attenuation of species concentration due to stronger destructive reactions. Furthermore, MHD convection in porous media has been a focal point in works like Yedhiri et al. [11], Ayub et al. [12], and Raju et al. [13] have examined the effects of thermal radiation and internal heat generation on the MHD flow of Casson fluids within a rotating porous medium. Their study focuses on flow induced by an inclined, oscillating vertical plate an arrangement that closely represents practical applications like oscillatory pumps and industrial separators. Chandra Sekhar and Vijaya Kumar [14] discussed how increasing the chemical reaction parameter leads to significant attenuation of species concentration. Islam and Hossain [15], who demonstrated that an increase in the radiation parameter leads to a decrease in temperature gradients, thus influencing the buoyancy-driven flow behaviour. These thermal effects become more complex when heat generation or absorption is introduced simultaneously, as shown by Goud and Reddy [16], Kavitha and Angel [17].

Gokulavani et al. [18], who studied the effects of permeability, Hall currents, and nanofluid properties on boundary layer characteristics. The role of the porous matrix in regulating momentum and thermal dispersion is crucial for applications such as underground thermal storage, insulation materials, and biological transport processes. Tetbirt et al. [19] conducted a comprehensive numerical evaluation of MHD mixed-convection and the heat mobility involving immiscible micropolar along with nanofluids within a vertical channel under a transverse magnetic field. The authors incorporated critical physical mechanisms, including Brownian motion, thermophoresis, magnetic forces, and microrotation, illustrating their combined effects on velocity, temperature, and nanoparticle concentration profiles.

Bormudoi and Ahmed [20] carried out a seminal investigation into unsteady MHD free-convective flow over a vertical plate subjected to parabolic ramped temperature and concentration boundary conditions. In addition, their model incorporates both the Soret (thermal diffusion) effect and the presence of an internal heat sink. Employing the Rosseland approximation for radiation and the Boussinesq assumption for buoyancy, they solved the governing non-linear partial differential equations using similarity transformations coupled with analytical techniques. Their results demonstrate notable transient behavior in velocity, temperature, and concentration fields, with ramped boundary conditions inducing time-dependent acceleration and deceleration of flow. Sakthivel and Sivakami [21], discussed an analytical solution of unsteady MHD immiscible fluid with chemical reaction in a porous medium under heat source.

Patoliya and Gohil [22] studied the chemical reaction on MHD Casson fluid flow past an oscillating plate in porous medium with hall current effects, analytical and numerical methods are used to analyze the fluid behavior. More recently, Kesavarani and Lakshmi Priya [23] studied the unsteady MHD oscillatory flow in a two-phase channel, focusing on the influence of the Soret effect (thermal diffusion) and oscillation-induced mixing. Their results highlight the significant impact of Soret-driven mass transport on the concentration and velocity profiles, particularly under varying thermal conditions. Raptis and Perdikis [24] presented one of the earliest analytical treatments of unsteady free convection in a highly porous medium under the influence of thermal radiation. Their findings demonstrated that radiation enhances the velocity and temperature fields, particularly in media with strong radiative absorption.

Balarabe et al. [25] analyzed the MHD heat and mass transfer characteristics of a second-grade fluid in the presence of thermal radiation. Their study emphasized the role of viscoelasticity and radiation in altering flow resistance and thermal distribution. Complementing this, Sinha and Choudhury [26] investigated the behavior for the flow of the MHD fluid past a vertical permeability plate under the influence of a heat source, providing insights into how internal heat generation affects both the thermal and momentum boundary layers.

While the previous studies haven't systematically examined Pressure and Heat Source in an Unsteady MHD Flow. This study examines it, along with the effects of permeability, radiative heat transfer, and chemical reaction of Newtonian fluid across an oscillating, vertically, infinite, permeable plate. that is located inside a highly saturated porous medium, with changing mass diffusion.

2. CONSTRUCTION AND RESOLUTION OF THE PROBLEM

Figure 1 illustrates the unsteady MHD laminar boundary flow of a viscous, Newtonian, incompressible fluid in an immeasurable vertical plate moving upwards through a porous layer. Coordinate system is defined such a way that the x-axis runs along the vertical direction of the plate's motion, while z-axis is normal to the plate's surface. Initially, both the fluid and the plate are at a uniform temperature T_∞ and solute concentration C_∞ , maintaining thermal and concentration equilibrium. At time t>0, the plate begins to move in its own plane with a velocity of $U_0 e^{i\omega t}$. Simultaneously, the surface temperature of the plate increases with time. A uniform magnetic field of strength B_0 is applied transversely to the plate. Due to the assumption of a low magnetic Reynalds number, the induced magnetic field is very small. The chemical reaction is assumed to be first-order, where the reaction rate is proportional to the deviation of concentration from its ambient value. The fluid is assumed to be gray, non-scattering, and capable of absorbing and emitting thermal radiation without any scattering effects. The Boussinesq approximation is applied, allowing density variations only in the buoyancy term of the momentum equation [1].

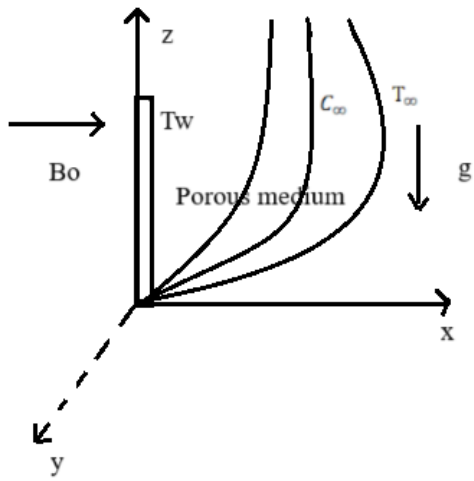

Figure 1. The problem's flow geometry

Then by Boussinesq approximation, the flow is ruled by the following:

$$\frac{\partial u^I}{\partial \mathrm{t}} = v\frac{\partial^2 u^I}{\partial \mathrm{z}^2} - \left(\frac{\sigma \mathrm{B}_0^2}{\rho} + \frac{v}{\mathrm{k}}\right)u^I + \mathrm{g}\beta(T^I - T_\infty^I) + \mathrm{g}\beta(C^I - C_\infty^I) - \frac{\partial P}{\partial \mathrm{z}} \tag{1}$$

$$\frac{\partial v^I}{\partial \mathrm{t}} = v\frac{\partial^2 u^I}{\partial \mathrm{z}^2} - \left(\frac{\sigma \mathrm{B}_0^2}{\rho} + \frac{v}{\mathrm{k}}\right)v^I \tag{2}$$

$$\rho \mathrm{C_p}\frac{\partial T^I}{\partial \mathrm{t}} = \mathrm{k}_1\frac{\partial^2 T^I}{\partial \mathrm{z}^2} - \frac{\partial \mathrm{qr}^2}{\partial \mathrm{z}} + \mathrm{Q_s}(T^I - T_\infty^I) \tag{3}$$

$$\frac{\partial C^I}{\partial \mathrm{t}} = \mathrm{D}\frac{\partial^2 C^I}{\partial \mathrm{z}^2} - Kr(C^I - C_\infty^I) \tag{4}$$

$$\begin{gathered} u^I = 0, v^I = 0, T^I = T_\infty^I, C^I = C_\infty^I, t \le 0; \\ \forall z u^I = \mathrm{U_0 e^{i\omega t}}, v^I = 0, T^I = T_\infty^I + (T_w^I - T_\infty^I) \\ \text{At } C^I = C_\infty^I + (C_w^I - C_\infty^I)A'\mathrm{t}, \text{ for } \mathrm{t} > 0; z = 0 \\ u^I \to 0, v^I \to 0, T^I \to T_\infty^I, C^I \to C_\infty^I, \text{ for } t > 0 \\ \text{as } z \to \infty \end{gathered} \tag{5}$$

Eqs. (1) and (2), let $q^I = u^I + \mathrm{i}v^I$, it is obtained as:

$$\frac{\partial q^I}{\partial \mathrm{t}} = v\frac{\partial^2 q^I}{\partial \mathrm{z}^2} - \left(\frac{\sigma \mathrm{B}_0^2}{\rho} + \frac{v}{\mathrm{k}}\right) q^I + \mathrm{g}\beta(T^I - T_\infty^I) + \mathrm{g}\beta(C^I - C_\infty^I) \tag{6}$$

When considering a gray, optically dense gas, the local radiative absorption is specified as:

$$\frac{\partial q^I}{\partial z} = -4a\sigma(T_\infty^{I4} - T^{I4}) \tag{7}$$

Raptis and Perdikis [24] consider that the flow variations in the temperature are limited enough. Let's assume that the temperature variations along the flow route are sufficiently minimal that T^{I4} within the free stream thermal T_∞^I using Taylor's series without accounting for higher-level variations. This yields the subsequent approximated performance:

$$T^{I4} \cong 4T_\infty^{I3}T^I - 3T_\infty^{I4} \tag{8}$$

$$\rho \mathrm{C_p}\frac{\partial T^I}{\partial \mathrm{t}} = \mathrm{k_1}\frac{\partial^2 T^I}{\partial \mathrm{z}^2} - 16\mathrm{a}\sigma\mathrm{T}_\infty^3(T^I - T_\infty^I) \tag{9}$$

The nondimensional quantities:

$$\begin{aligned}&\mathrm{z}'' = \frac{\omega_0 \mathrm{z}}{v}, \frac{\partial q^I}{\partial z} = \frac{q'}{\mathrm{U_0}}, \theta^I = \frac{T' - \mathrm{T}_\infty}{\mathrm{T_w} - \mathrm{T}_\infty}, \mathrm{Pr} = \frac{\rho v \mathrm{C_p}}{\mathrm{k_1}}, \mathrm{K} = \frac{\mathrm{U_0^2 k}}{v^2},\\ &\mathrm{P} = \frac{-\mathrm{h}^2}{\mu u^I}\left(\frac{\partial \mathrm{P}}{\partial \mathrm{Z}}\right), \mathrm{Sc} = \frac{\mathrm{v}}{\mathrm{D}}, \phi^I = \frac{\mathrm{C} - \mathrm{C}_\infty}{\mathrm{C_w} - \mathrm{C}_\infty}, \mathrm{M}^2 = \frac{\sigma v \mathrm{B_0^2}}{\rho \mathrm{U_0^2}}, \mathrm{R} =\\ &\frac{16\mathrm{av}\sigma\mathrm{T}_\infty^3}{\mathrm{k_1 U_0^2}}, \mathrm{Gm} = \frac{v\mathrm{g}\beta(\mathrm{C_w} - \mathrm{C}_\infty)}{\mathrm{U_0^3}}, \mathrm{Gr} = \frac{v\mathrm{g}\beta(\mathrm{T_w} - \mathrm{T}_\infty)}{\mathrm{U_0^3}}, \mathrm{Kr} = \frac{\mathrm{vK_1}}{\mathrm{v_w^2}},\\ &\mathrm{A} = \frac{\mathrm{U_0^2}}{v}, \mathrm{t}'' = \frac{\mathrm{U_0^2 t}}{v}, \mathrm{N} = \mathrm{M}^2 + \frac{1}{\mathrm{K}}, Q = \frac{Qsv}{\rho c_p U_0}\end{aligned} \tag{10}$$

By the transformation of Eq. (10), the nondimensional form of Eqs. (1), (4), and (9) are:

$$\frac{\partial \mathrm{q^I}}{\partial \mathrm{t}} = \frac{\partial^2 \mathrm{q^I}}{\partial \mathrm{z}^2} - \mathrm{Nq^I} + \mathrm{Gr}\theta^\mathrm{I} + \mathrm{Gm}\phi^\mathrm{I} - \mathrm{P} \tag{11}$$

$$\frac{\partial \theta^I}{\partial t} = \frac{1}{\mathrm{Pr}}\frac{\partial^2 \theta^I}{\partial z^2} - \frac{R}{Pt}\theta^I + Q\theta^I \tag{12}$$

$$\frac{\partial \phi^\mathrm{I}}{\partial \mathrm{t}} = \frac{1}{\mathrm{Sc}}\frac{\partial^2 \phi^\mathrm{I}}{\partial \mathrm{z}^2} - \mathrm{Kr}\phi^\mathrm{I} \tag{13}$$

Initial boundary conditions [1]:

$$\begin{aligned}&q^I = 0, \theta^I = 0, \phi^I = 0, t \le 0; \forall z\\ &q^I = e^{i\omega t}, \theta^I = t, \phi^I = t, t > 0; \text{ at } z = 0\\ &q^I \to 0, \theta^I \to 0, \phi^I \to 0, t > 0; \text{ as } z \to \infty.\end{aligned} \tag{14}$$

The solution of concentration, temperature, and velocity distributions is obtained by mathematically solving the uncertain coupled differential equations with partial solutions. Eqs. (11)-(13) and the resulting boundary conditions (Eq. (14)) use the Laplace transformation approach, considering Eq. (13) and taking Laplace on both sides.

Using Laplace expansion:

$$\mathrm{L}\left[\frac{\partial \phi^\mathrm{I}}{\partial \mathrm{t}}\right] = \frac{1}{\mathrm{Sc}}\mathrm{L}\left[\frac{\partial^2 \phi^\mathrm{I}}{\partial \mathrm{z}^2}\right] - \mathrm{KrL}[\phi^\mathrm{I}] \tag{15}$$

$$\frac{1}{\mathrm{Sc}}\frac{\mathrm{d}^2\overline{\phi^\mathrm{I}}}{\mathrm{dz}^2} - \mathrm{Kr}\overline{\phi^\mathrm{I}} - \mathrm{s}\overline{\phi^\mathrm{I}} = 0 \tag{16}$$

Then we get:

$$\bar{\phi}_{(z,s)} = C_1 e^{-(\sqrt{Kr \cdot Sc + s \cdot Sc})z} + C_2 e^{(\sqrt{Kr \cdot Sc + s \cdot Sc})z} \tag{17}$$

Then obtain $\mathrm{C_1}$ and $\mathrm{C_2}$ value using boundary conditions, $\mathrm{C_1} = \frac{1}{\mathrm{s}^2}$ and $\mathrm{C_2} = 0$. Substituting $\mathrm{C_1}$, $\mathrm{C_2}$ in Eq. (17).

$\bar{\Phi}_{(\mathrm{z,s})} = \frac{\mathrm{e}^{-(\sqrt{\mathrm{Kr \cdot Sc + s \cdot Sc}})\mathrm{z}}}{\mathrm{s}^2}$, now taking inverse Laplace transform we get Eq. (18).

$$\phi^\mathrm{I} = \left(\left(\frac{\mathrm{t}}{2} + \frac{\mathrm{Z}\sqrt{\mathrm{Sc}}}{4\sqrt{\mathrm{Kr}}}\right)\exp\left(\mathrm{Z}\sqrt{\mathrm{Kr} \cdot \mathrm{Sc}}\right)\mathrm{erfc}(\eta\sqrt{\mathrm{Sc}} + \sqrt{\mathrm{Kr} \cdot \mathrm{t}})\right) + \left(\left(\frac{\mathrm{t}}{2} - \frac{\mathrm{Z}\sqrt{\mathrm{Sc}}}{4\sqrt{\mathrm{Kr}}}\right)\exp\left(-\mathrm{Z}\sqrt{\mathrm{Kr} \cdot \mathrm{Sc}}\right)\mathrm{erfc}(\eta\sqrt{\mathrm{Sc}} - \sqrt{\mathrm{Kr} \cdot \mathrm{t}})\right) \tag{18}$$

$$\theta^I = \left(\left(\frac{t}{2} + \frac{Z\sqrt{\mathrm{Pr}}}{4\sqrt{B}}\right)\exp\left(Z\sqrt{B \cdot \mathrm{Pr}}\right)\mathrm{erfc}(\eta\sqrt{\mathrm{Pr}} + \sqrt{B \cdot t})\right) + \left(\left(\frac{t}{2} - \frac{Z\sqrt{\mathrm{Pr}}}{4\sqrt{B}}\right)\exp\left(-Z\sqrt{B \cdot \mathrm{Pr}}\right)\mathrm{erfc}(\eta\sqrt{\mathrm{Pr}} - \sqrt{B \cdot t})\right) \tag{19}$$

$$\begin{aligned}\mathrm{Q^I} = {} & \tfrac{1}{2}\exp\left(\tfrac{1+\mathrm{i}\omega}{\mathrm{N}}\right)\mathrm{t}\left\{\exp\left(-\mathrm{Z}\sqrt{(1+\mathrm{i}\omega)}\right)\mathrm{erfc}(\eta\sqrt{\mathrm{N}} - \sqrt{\left(\tfrac{1+\mathrm{i}\omega}{\mathrm{N}}\right)\mathrm{t}}) + \exp\left(\mathrm{Z}\sqrt{(1+\mathrm{i}\omega)}\right)\mathrm{erfc}\left(\eta\sqrt{\mathrm{N}} + \sqrt{\left(\tfrac{1+\mathrm{i}\omega}{\mathrm{N}}\right)\mathrm{t}}\right)\right\}\\ & + \frac{\mathrm{D}}{\mathrm{k_1^2}}\left\{\left(\frac{1}{2}\exp\left(\frac{\mathrm{K_2}}{\mathrm{Pr}}\right)\mathrm{t}\right)\left[\exp\left(-\mathrm{Z}\sqrt{\mathrm{K_2}}\right)\mathrm{erfc}\left(\eta\sqrt{\mathrm{Pr}} - \sqrt{\left(\frac{\mathrm{K_2}}{\mathrm{Pr}}\right)\mathrm{t}}\right) + \exp\left(\mathrm{Z}\sqrt{\mathrm{K_2}}\right)\mathrm{erfc}\left(\eta\sqrt{\mathrm{Pr}} + \sqrt{\left(\frac{\mathrm{K_2}}{\mathrm{Pr}}\right)\mathrm{t}}\right)\right]\right\}\\ & + \sqrt{\mathrm{k1}}\left\{\left(\frac{\mathrm{t}}{2} + \frac{\mathrm{ZPr}}{4\sqrt{\mathrm{K_2}}}\right)\left[\exp\left(\mathrm{Z}\sqrt{\mathrm{K_2}}\right)\mathrm{erfc}\left(\frac{\mathrm{z}\sqrt{\mathrm{Pr}}}{2\sqrt{\mathrm{t}}} + \sqrt{\left(\frac{\mathrm{K_2}}{\mathrm{Pr}}\right)\mathrm{t}}\right) + \exp\left(\frac{\mathrm{t}}{2} + \frac{\mathrm{ZPr}}{4\sqrt{\mathrm{K_2}}}\right)\exp\left(-\mathrm{Z}\sqrt{\mathrm{K_2}}\right)\mathrm{erfc}\left(\frac{\mathrm{Z}\sqrt{\mathrm{Pr}}}{2\sqrt{\mathrm{t}}} + \sqrt{\left(\frac{\mathrm{K_2}}{\mathrm{Pr}}\right)\mathrm{t}}\right)\right]\right\}\\ & + \frac{\mathrm{D}}{\mathrm{k_1^2}}\left\{\left(\frac{1}{2}\exp\left(\frac{\mathrm{K_2}}{\mathrm{Pr}} + \mathrm{K_1}\right)\mathrm{t}\right)\left[\exp\left(-\mathrm{Z}\sqrt{\left(\frac{\mathrm{K_2}}{\mathrm{Pr}} + \mathrm{K_1}\right)}\mathrm{Pr}\right)\mathrm{erfc}\left(\eta\sqrt{\mathrm{Pr}} - \sqrt{\left(\frac{\mathrm{K_2}}{\mathrm{Pr}} + \mathrm{K_1}\right)\mathrm{t}}\right) + \exp\left(\mathrm{Z}\sqrt{\left(\frac{\mathrm{K_2}}{\mathrm{Pr}} + \mathrm{K_1}\right)\mathrm{Pr}}\right)\mathrm{erfc}\left(\eta\sqrt{\mathrm{Pr}} + \sqrt{\left(\frac{\mathrm{k_2}}{\mathrm{Pr}} + \mathrm{K_1}\right)\mathrm{t}}\right)\right]\right\}\\ & - \frac{\mathrm{F}}{\mathrm{K_3^2}}\left\{\left(\frac{1}{2}\exp(\mathrm{Kr} \cdot \mathrm{t})\right)\left[\exp\left(-\mathrm{Z}\sqrt{\mathrm{Kr} \cdot \mathrm{Sc}}\right)\mathrm{erfc}(\eta\sqrt{\mathrm{Sc}} - \sqrt{\mathrm{Kr} \cdot \mathrm{t}}) + \exp\left(\mathrm{Z}\sqrt{\mathrm{Kr} \cdot \mathrm{Sc}}\right)\mathrm{erfc}(\eta\sqrt{\mathrm{Sc}} + \sqrt{\mathrm{Kr} \cdot \mathrm{t}})\right]\right\}\\ & + \frac{\mathrm{F}}{\mathrm{K_3}}\left\{\left(\frac{\mathrm{t}}{2} + \frac{\mathrm{Z}}{4}\sqrt{\frac{\mathrm{Sc}}{\mathrm{Kr}}}\right)\left[\exp\left(\mathrm{Z}\sqrt{\mathrm{Sc} \cdot \mathrm{Kr}}\right)\mathrm{erfc}\left(\eta\sqrt{\mathrm{Sc}} + \sqrt{\mathrm{Kr} \cdot \mathrm{t}}\right) + \left(\frac{\mathrm{t}}{2} - \frac{\mathrm{z}}{4}\sqrt{\frac{\mathrm{Sc}}{\mathrm{Kr}}}\right)\exp\left(-\mathrm{Z}\sqrt{\mathrm{Sc} \cdot \mathrm{Kr}}\right)\mathrm{erfc}\left(\eta\sqrt{\mathrm{Sc}} - \sqrt{\mathrm{Kr} \cdot \mathrm{t}}\right)\right]\right\}\\ & + \frac{\mathrm{F}}{\mathrm{K_3^2}}\left\{\frac{1}{2}\exp\left(\mathrm{Kr} - \mathrm{K_2}\right)\mathrm{t}\left[\exp\left(-\mathrm{Z}\sqrt{(\mathrm{Kr} - \mathrm{K_3})\mathrm{Sc}}\right)\mathrm{erfc}(\eta\sqrt{\mathrm{Sc}} - \sqrt{(\mathrm{Kr} - \mathrm{K_3})\mathrm{t}}) + \exp\left(\mathrm{Z}\sqrt{(\mathrm{Kr} - \mathrm{K_3})\mathrm{Sc}}\right)\mathrm{erfc}(\eta\sqrt{\mathrm{Sc}} + \sqrt{(\mathrm{Kr} - \mathrm{K_3})\mathrm{t}})\right]\right\}\end{aligned} \tag{20}$$

3. RESULT AND DISCUSSION

The impact of the non-coupling parameters with radiation parameter (R), dimensionless time (t), and permeable parameter (K) along with Hartmann number (M) and Grashof number (Gr), on the velocity component velocity q^I , temperature θ^I, and concentration ϕ^I has been numerically assessed. It explores the concentration, velocity, and temperature identities by altering variables by keeping the parameters fixed as the Grashof number (Gr=3), Gm=3>0, Prandtl number (Pr=0.71), Schmidt volume (Sc=0.22), Heat source (Qs=0.05), K=2, P=0.2, and M=0.5, the profile is plotted by varying one parameter at a time while holding the others constant. We employed MATLAB to collect and analyze the data.

According to Figure 2, the graphic illustrates that concentration diminishes as the Schmidt number (Sc) increases. Physically, this is accurate, as an increase in Sc results in a reduction of molecular diffusivity, thus leading to reduced concentrations at the edge of the layer. Consequently, low Sc values elevate the species concentration, while high Sc values diminish it. Figure 3 illustrates that how chemical reaction affects the concentration profile if destructive chemical reaction increasing the reaction rate leads to lower concentration, because more solute is consumed by the reaction. The concentration is observed to increase during time t as shown in Figure 4. Figure 5 illustrates the transient temperature distribution with respect to z. The temperature attains its extreme value gradually decreases to zero as the distance increase. The temperature magnitude is higher for air (Pr=0.71) compared to water (Pr=7), which is particularly attributed to the drop in thermal conductivity with increasing Prandtl number. Figure 6 illustrates the radiation variable, the radiation parameter (R) of the temperature profiles shows a minor decrease in association with the thermal conductivity ratio, which increases with the magnitude of the radiation factor this is due to the radiating effect, which causes the gas to transmit heat onto the surface. The gas or liquid gets more viscous as a result of its temperature dropping. Figure 7 illustrates how Qs affects temperature profiles. It is evident that due to the added heat energy impacts the temperature profile proportionally.

Figure 8 shows the influence of the temperature Grashof number (Gr) with the velocity gradient. The study implicates the increase in Gr correlates with a rise in acceleration. In Figure 9, the mass Grashof number (Gm) dictates the relationship between buoyant and viscous dynamical forces. As the buoyancy force of a species intensifies, fluid velocity diminishes, resulting in a more pronounced peak value. The range of velocity attains its maximum near the plate before progressively diminishing to the empty stream frequency, on the field of motion. The velocity increases in association with increasing Solutal Grashof quantity ranges.

As Pr increases, velocity component decreases (Figures 10-11). Moreover, the acceleration diminishes and approaches its smallest value near the plate. The velocity components diminish as the Schmidt ratio (Sc) increases. Figure 12 illustrates an increase in the radiation parameter (R) velocity component as it decreases, because radiation damps the temperature field, thereby weakening buoyancy driven flow which reduces the overall fluid acceleration.

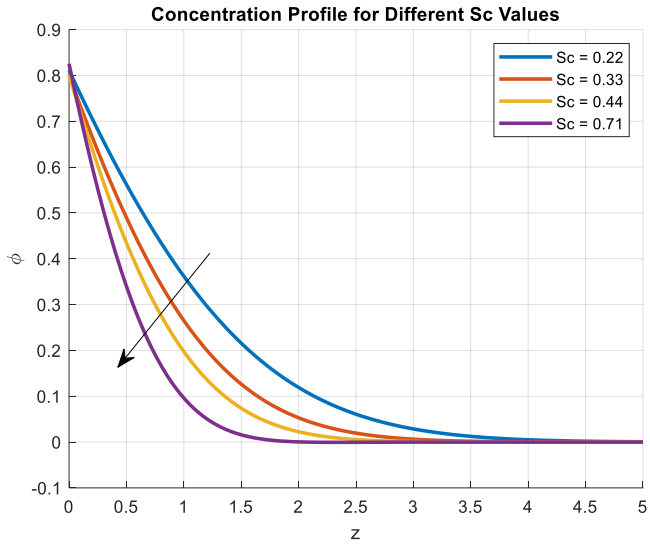

Figure 2. Influence of the Schmidt number (Sc) for concentration

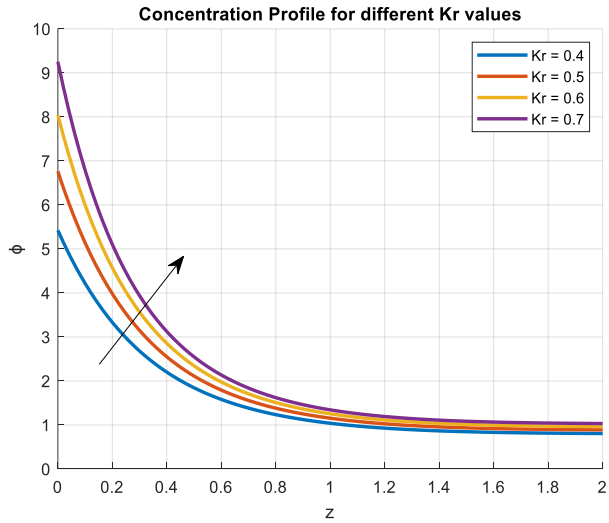

Figure 3. Influence of the chemical reaction (Kr) for concentration

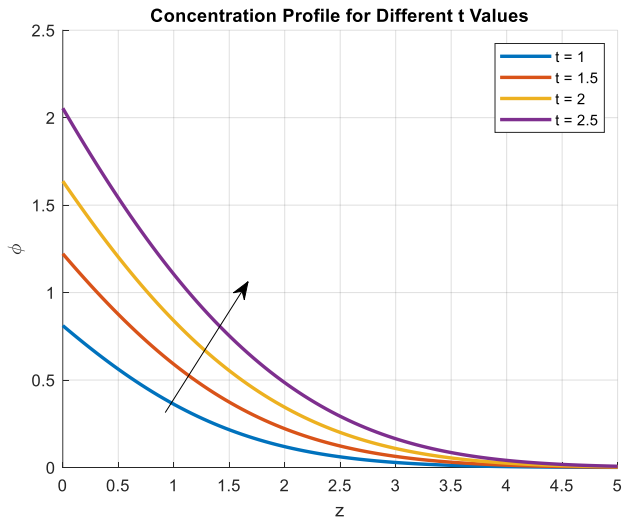

Figure 4. Influence of time for the concentration profile

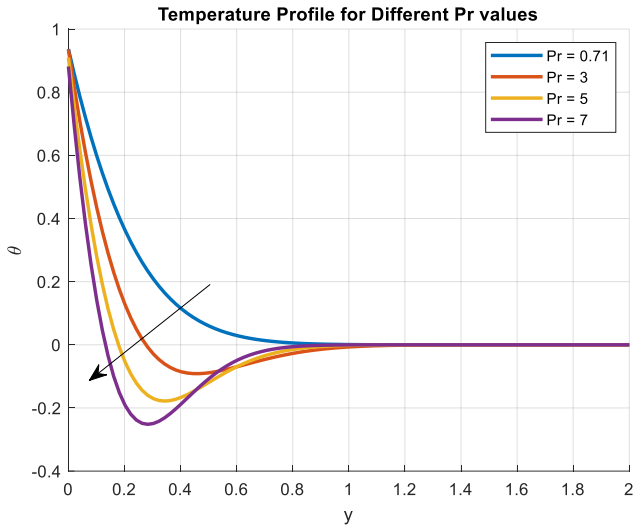

Figure 5. Influence of Prandtl number (Pr) for the temperature profile

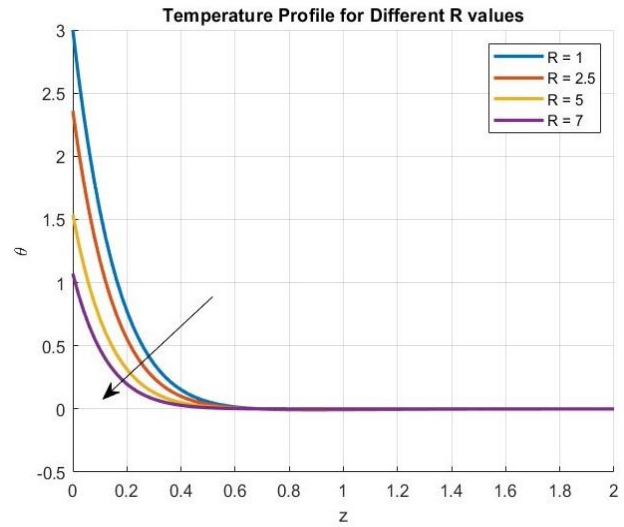

Figure 6. Consequence of Radiation parameter (R) for the temperature

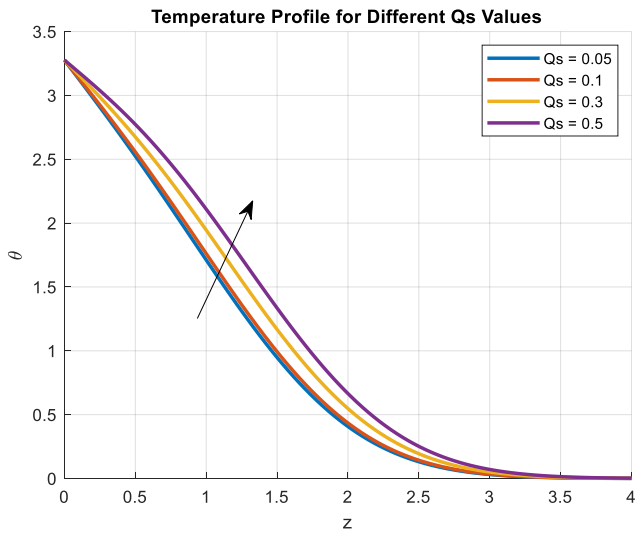

Figure 7. Impression of Heat source (Qs) for the temperature profile

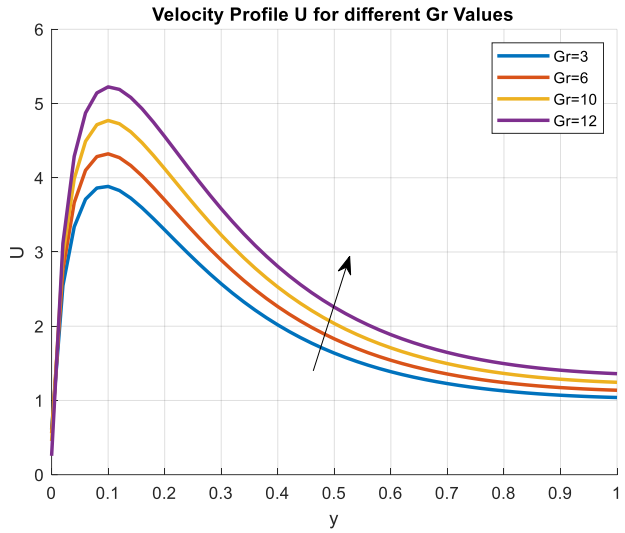

Figure 8. Influence of the Grashof number (Gr) for velocity

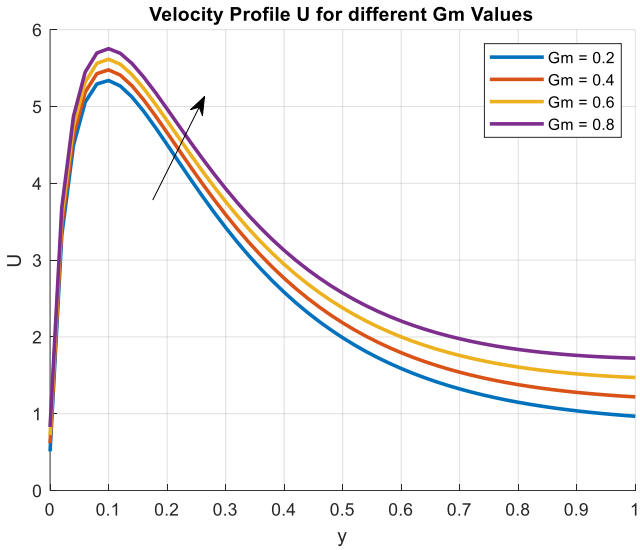

Figure 9. Effect of the Grashof number (Gm) for velocity

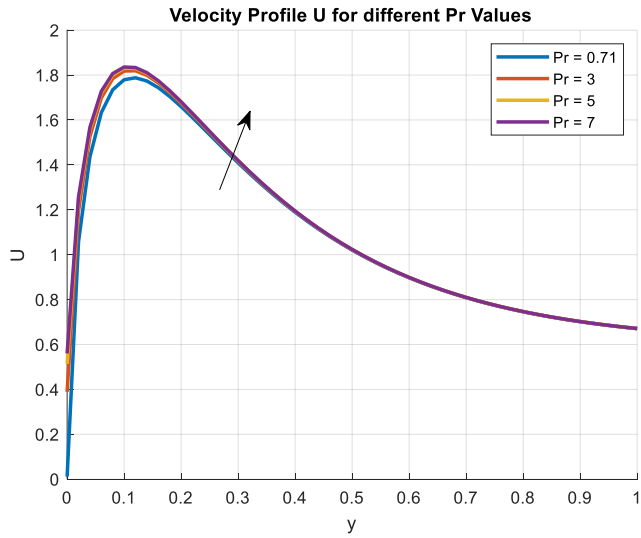

Figure 10. Effect of the Prandtl number (Pr) for the velocity

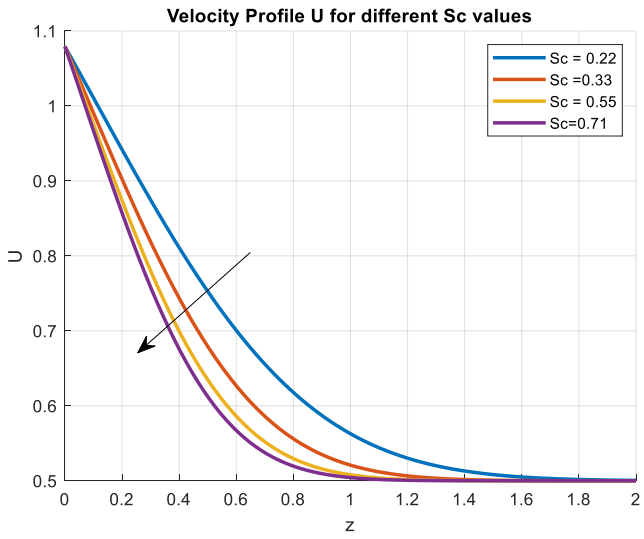

Figure 11. Influence of Schmidt number (Sc) for the velocity

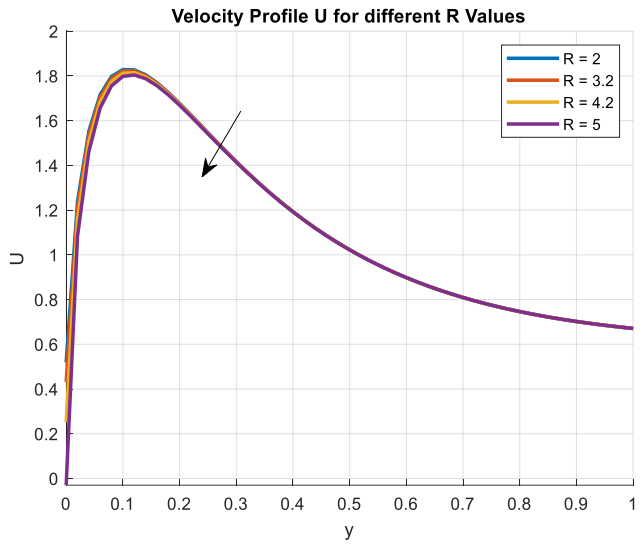

Figure 12. Influence of Radiation parameter (R) for the velocity

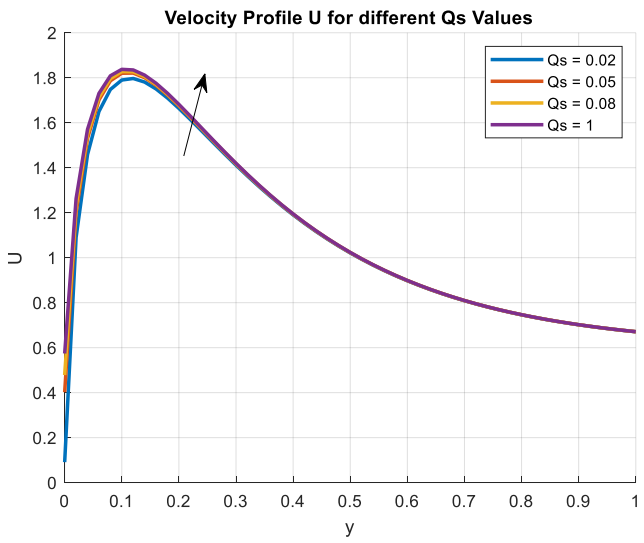

Figure 13. Effect of Heat source (Qs) for the velocity profile

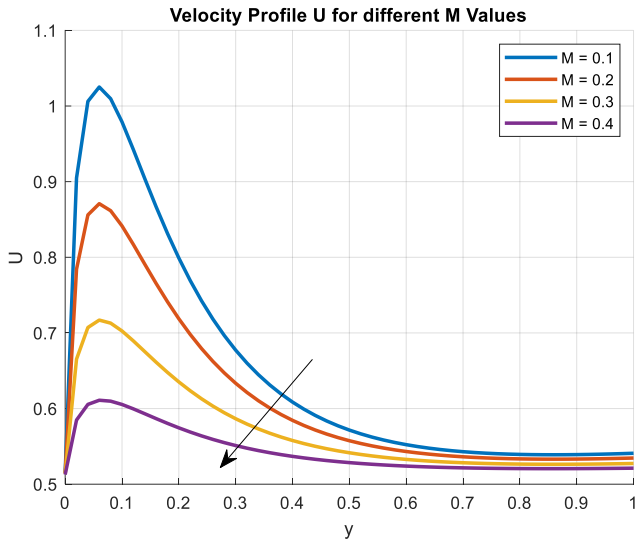

Figure 14. Influence of Magnetic parameter (M) for the velocity

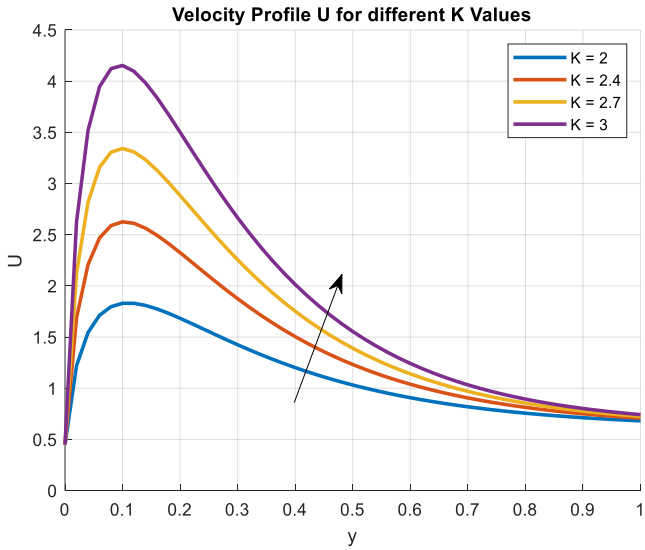

Figure 15. Effect of Porous parameter (K) for the velocity

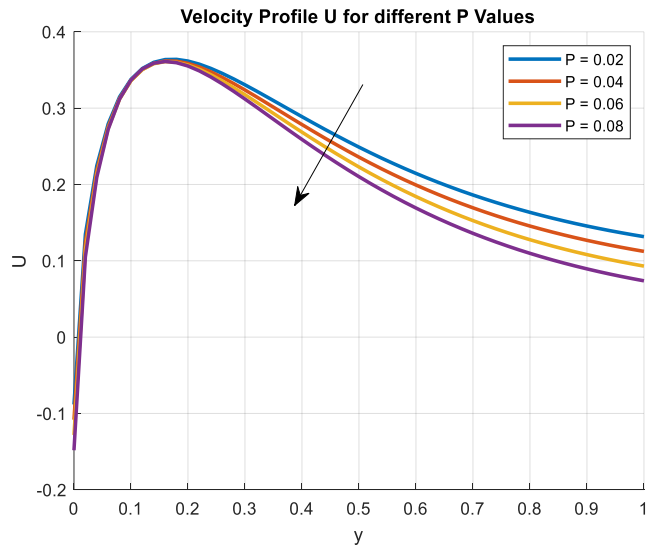

Figure 16. Effect of Pressure (P) for the velocity profile

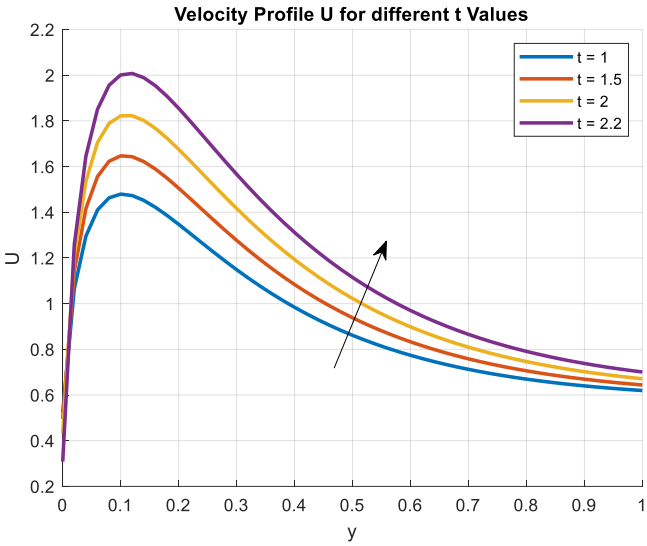

Figure 17. Influence of time parameter (t) for the velocity profile

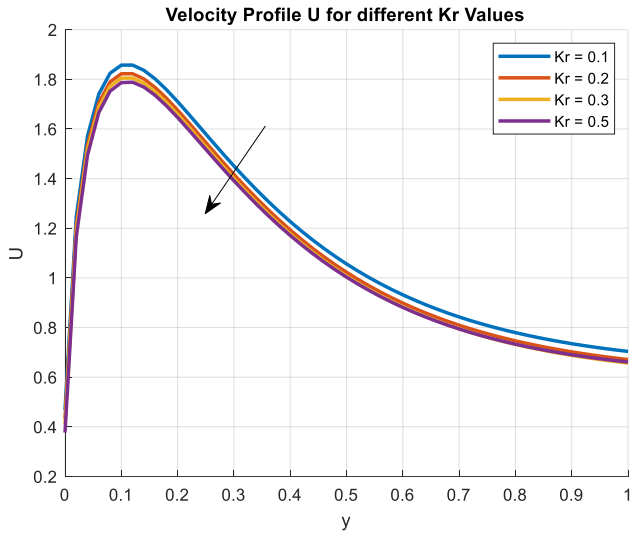

Figure 18. Influence of chemical reaction (Kr) for the velocity

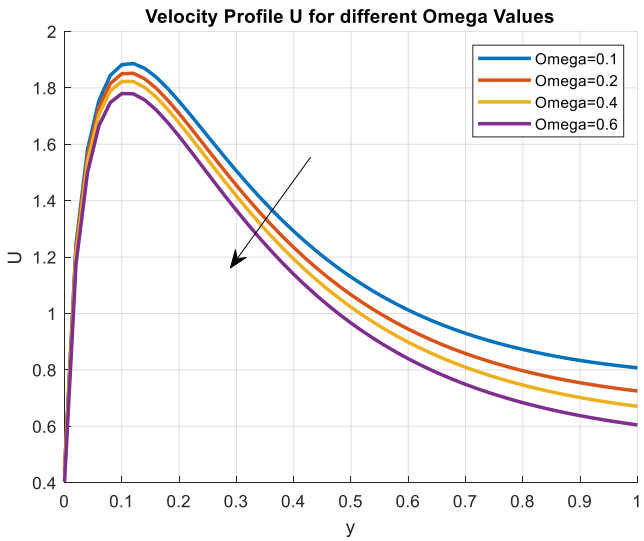

Figure 19. Effect of oscillating parameter (ω) for the velocity profile

In Figure 13, on Qs for velocity profiles this graphic illustrates whether the generation of heat enhances the buoyancy force, resulting in an increased flow rate and subsequently elevated acceleration profiles. The velocity features in Figure 14 exhibit a retardation as the magnetic force amplitude (Hartmann number M) increases. It is evident that acceleration decreases at all sites when the regional magnetic factor M increases. The imposition of a longitudinal magnetic field on an electrically conductor fluid generates a resistance force known as the Lorentz force.

Figure 15 demonstrates how the velocity components vary as the permeability parameter K changes. As the permeability parameter K increases, the velocity components get higher. The flow velocity diminishes when a porous material is present because it raises the resistance to flow. The velocity's decline with decreasing K exhibits this behaviour. Figure 16 indicates the way pressure affects the acceleration profile; as the pressure level rises, so does the velocity profile decreases. As pressure increases along the direction of flow, the velocity profile decreases due to the opposing pressure force acting against the fluid motion. Figure 17 shows an increase in velocity as time t passes. Figure 18 illustrates how the velocity fields are affected by the chemical reaction parameter Kr. These numbers show that the velocity fields decrease as Kr rises due to enhanced resistance in the flow field caused by the interaction of chemical species. According to physical principles, the flow field naturally decreases as Kr increases. Lastly, Figure 19 reveals that velocity increases as oscillation frequency ω increases. Table 1 illustrates the comparison result of the previous work carried out by Krishna et al. [1] and the present study. Where in addition with heat source leads to a slight but consistent increase in temperature profile. Which correlates with the existing system.

Table 1. Comparison of results for temperature profile

Pr	Previous Result [1] Laplace Transform Technique	Present Results Laplace Transform Technique, Adding Qs
0.71	0.0711681	0.0711772
3	0.0025271	0.0025401
7	0.0000186	0.0000192

4. CONCLUSIONS

Using a flux model, we have reproduced the effects of heat radiation in very dense gases. The following conclusions are obtained by applying the Laplace transform methodology with appropriate bounds to the analytical results of the governing equations:

(1). The velocity frequently diminishes with a rise in Hartmann's number M. and oscillation ω decreases in the velocity flow.

(2). When Grashof number, Gr and Gc, increase velocity gradually increases. Which increases buoyancy forces, and fluid flow rises.

(3). As time increases, the velocity, temperature, and concentration are increasingly enhanced.

(4). The acceleration and temperature fluctuated with variations in the free convection-radiation factor.

(5). A rise in Sc along with time results in a progressive acceleration of the energy transfer coefficient.

(6). As chemical reaction Kr rises the velocity profile reduced, and concentration increases.

(7). As heat source Qs moves up as the velocity increase and temperature decrease.

REFERENCES

[1] Krishna, M.V., Reddy, M.G., Chamkha, A.J. (2021). Heat and mass transfer on unsteady MHD flow through an infinite oscillating vertical porous surface. Journal of Porous Media, 24(1): 81-100. http://doi.org/10.1615/JPorMedia.2020025021

[2] Krishna, M.V., Chamkha, A.J. (2020). Hall and ion slip effects on unsteady MHD convective rotating flow of nanofluids—Application in biomedical engineering. Journal of the Egyptian Mathematical Society, 28(1): 1-15. https://doi.org/10.1186/s42787-019-0065-2

[3] Krishna, M.V. (2020). Hall and ion slip impacts on unsteady MHD free convective rotating flow of Jeffreys fluid with ramped wall temperature. International Communications in Heat and Mass Transfer, 119: 104927. http://doi.org/10.1016/j.icheatmasstransfer.2020.104927

[4] Krishna, M.V., Chamkha, A.J. (2019). Hall and ion slip effects on MHD rotating boundary layer flow of nanofluid past an infinite vertical plate embedded in a porous medium. Results in Physics, 15: 102652. http://doi.org/10.1016/j.rinp.2019.102652

[5] Krishna, M.V., Jyothi, K. (2018). Hall effects on MHD rotating flow of a visco-elastic fluid through a porous medium over an infinite oscillating porous plate with heat source and chemical reaction. Materials Today: Proceedings, 5(1): 367-380. http://doi.org/10.1016/j.matpr.2017.11.094

[6] Khanam, M., Ahmed, N. (2024). MHD nonlinear natural convection from a uniformly moving porous vertical plate with constant heat and mass flux in the presence of thermal radiation, diffusion-thermo, heat sink, and chemical reaction. Heat Transfer, 53(2): 867-892. http://doi.org/10.1002/htj.22979

[7] Anand Kumar, S.A., Sreedhar, S., Veera Krishna, M. (2024). Heat and mass transfer on unsteady MHD convective flow through porous medium between two vertical plates with chemical reaction. Proceedings of the Institution of Mechanical Engineers, Part E: Journal of Process Mechanical Engineering, 238(4): 1665-1675. https://doi.org/10.1177/09544089231160877

[8] Merkin, J.H., Roşca, N.C., Roşca, A.V., Pop, I. (2024). MHD mixed convection flow over a permeable vertical flat plate embedded in a Darcy–Forchheimer porous medium. Transport in Porous Media, 151(13): 2511-2528. https://doi.org/10.1007/s11242-024-02124-6

[9] Ahammad, N.A., Badruddin, I.A., Kamangar, S., Khaleed, H.M.T., Saleel, C.A., Mahlia, T.M.I. (2021). Heat transfer and entropy in a vertical porous plate subjected to suction velocity and MHD. Entropy, 23(8): 1069. http://doi.org/10.3390/e23081069

[10] Hari Babu, B. (2023). Heat and mass transfer on unsteady MHD Casson fluid flow past an infinite vertical porous plate with chemical reaction. Proceedings of the Institution of Mechanical Engineers, Part E: Journal of Process Mechanical Engineering, 237(6): 2278-2289. http://doi.org/10.1177/09544089221133966

[11] Yedhiri, S.R., Palaparthi, K.K., Kodi, R., Asmat, F. (2024). Unsteady MHD rotating mixed convective flow through an infinite vertical plate subject to Joule heating, thermal radiation, Hall current, radiation absorption. Journal of Thermal Analysis and Calorimetry, 149(16): 8813-8826. http://doi.org/10.1007/s10973-024-12954-7

[12] Ayub, R., Ahmad, S., Ahmad, M. (2022). MHD rotational flow of viscous fluid past a vertical plate with slip and Hall effect through porous media: A theoretical modeling with heat and mass transfer. Advances in Mechanical Engineering, 14(6): 16878132221103330. http://doi.org/10.1177/16878132221103330

[13] Raju, R., Selvaraj, A., Jose, S.D., Chithra, K. (2025). Effects of radiation and heat generation on MHD Casson fluid flowing in a porous medium rotating on an inclined oscillating vertical plate. JP Journal of Heat and Mass Transfer, 38(3): 315-339. http://doi.org/10.17654/0973576325016

[14] Chandra Sekhar, B., Vijaya Kumar, P. (2023). Chemical reaction impacts the unsteady MHD convective flow of an incompressible viscous fluid past an infinite vertical porous plate. Heat Transfer, 52(2): 1474-1496. http://doi.org/10.1002/htj.22751

[15] Islam, M.M., Hossain, R. (2024). Heat and mass transfer in unsteady MHD Casson fluid flow over a semi-infinite vertical plate through porous medium with dissipative and radiative effects. Sciences, 5: 6611-7687. http://doi.org/10.35940/ijisme.E7974.12111124

[16] Goud, B.S., Reddy, Y.D. (2022). Chemical reaction and Soret effect on an unsteady MHD heat and mass transfer fluid flow along an infinite vertical plate with radiation and heat absorption. Journal of the Indian Chemical Society, 99(11): 100762. https://doi.org/10.1016/j.jics.2022.100762

[17] Kavitha, R., Angel, J. (2025). Impact of rotation and chemical reactions on MHD mixed convection flow over an inclined heated porous plate with heat and mass transfer analysis. WSEAS Transactions on Fluid Mechanics, 20: 40-50. http://doi.org/10.37394/232013.2025.20.5

[18] Gokulavani, P., Muthukumar, S., Sureshkumar, S., Muthtamilselvan, M., Al-Mdallal, Q.M. (2025). Computational analysis of MHD flow in a porous open chamber filled with hybrid nanofluid and vertical heat sources. Journal of Thermal Analysis and Calorimetry, 150: 3621-3636. https://doi.org/10.1007/s10973-024-13892-0

[19] Tetbirt, A., Djebiret, M.A., Ouali, M., Mokrane, M., Bouaziz, M.N. (2024). Numerical investigation of MHD mixed-convective flow and heat transfer within immiscible micropolar and nanofluids in a vertical channel. International Journal of Modelling and Simulation, 1-22. http://doi.org/10.1080/02286203.2024.2315535

[20] Bormudoi, M., Ahmed, N. (2024). Study of an unsteady magnetohydrodynamic-free convective flow under parabolic ramped temperature and concentration in the presence of Soret and heat sink. Heat Transfer, 53(3): 1371-1391. http://doi.org/10.1002/htj.22995

[21] Sakthivel, P.R., Sivakami, L. (2024) Analytical solution of unsteady MHD immiscible fluid with thermal radiation and chemical reaction in a porous medium under heat source. Journal of Interdisciplinary Mathematics, 27(5): 1017-1027. http://doi.org/10.47974/JIM-1929

[22] Patoliya, R., Gohil, V. (2025). Chemical reaction and hall current effects on MHD Casson fluid flow past an

oscillating plate in porous medium. Advances in Nonlinear Variational Inequalities, 28(7s): 45-62. http://doi.org/10.52783/anvi.v28.4483

[23] Kesavarani, S., Lakshmi Priya, S. (2024). Soret-driven influence on unsteady magnetohydrodynamic mixed oscillatory flow in a two-phase channel: Exploring the thermal effects. Journal of Interdisciplinary Mathematics, 27(5): 1053-1065. http://doi.org/10.47974/JIM-1932

[24] Raptis, A., Perdikis, C. (2004). Unsteady flow through a highly porous medium in the presence of radiation. Transport in Porous Media, 57(2): 171-179. https://doi.org/10.1023/B:TIPM.0000038262.65594.e8

[25] Balarabe, A.Y., Danjumma, Y.I., Abubakar, G.A., Barga, Y.I. (2023). Unsteady MHD flow of heat and mass transfer for second grade fluid in the presence of thermal radiation. International Journal of Multidisciplinary Research and Growth Evaluation, 4(4): 122-128.

[26] Sinha, A., Choudhury, L. (2024). MHD flow from a vertical porous plate in presence of heat source. Asian Research Journal of Mathematics, 20(11): 177-186. https://doi.org/10.9734/arjom/2024/v20i11869

NOMENCLATURE

u,v	Velocity components
t	Dimensionless time
P	Pressure source
B_0	Coefficient of electromagnetic field
R	Thermal Radiation parameter
θ^I	Dimensionless temperature
K	Permeability parameter
k	Permeability of porous medium
v	Kinematic viscosity
μ	Fluid viscosity
g	Acceleration due to gravity
q^I	Velocity parameter
ϕ^I	Dimensionless concentration
T_W	Fluid temperature at plate
C_W	Fluid concentration at plate
Gr	Thermal Grashof number
Gc	Mass Grashof number
M	Hartmann number
Pr	Prandtl number
Sc	Schmidt number
α	Viscosity ratio
β	Coefficient of heat transfer
ρ	Density
σ	Electrical conductivity
ω	Frequency parameter
a	Spectral mean absorption coefficient of the medium
∞	free stream conditions
U_0	Dimensionless plate velocity
D	Chemical molecular diffusivity
C_p	Heat at constant pressure
Kr	Chemical reaction parameter
Qs	Heat source parameter